ISME

Modeling the Effects of Geometric Asymmetry on Aero-heating of the Ablative Noses

M. Mardani[*]
PhD Candidate

M. M. Doustdar[†]
Associate Professor

The purpose of the proposed research methodology is to improve the temperature contour calculations of aero-heating code (CTCA) for the Asymmetrical and non-circular ablative noses by using the equivalent axisymmetric body (EAB) theory. This Code has been developed by researchers and the results of it have been validated by the various flight tests results. In the case of non-zero angle of attack or asymmetric surface ablation for each meriodinal plane, the equivalent meriodinal plane (EMP) is created for any meriodinal plane. The combinations of these planes constitute the EAB. The governing equations are solved for this body by using the non-equilibrium chemical reactions and the results of it are mapped to the main body. The solving of a typical nose during flight trajectory show that the convergence of this technique is very fast as compare to the user defined function (UDF) based on the fluent solvers. The results of this research are validated by the UDF and the relative error of it is less than 10 percent.

Keywords : CTCA (Calculating of Temperature Contour and Aero-heating) Code, EAB (Equivalent Axisymmetric Body) Theory, EMP (Equivalent Meridional Plane), UDF (User Defined Function)

1 Introduction

The induced aero-heating on the windward side of a three-dimensional (3D) blunt body of the supersonic & hypersonic vehicles is caused by conversion of the flow kinetic energy to internal energy. The magnitude of this parameter depends on the thermodynamic properties of shock layer gas mixture, chemical reactions, surface ablation, surface friction, geometric asymmetry effects, and flight conditions. During flight trajectory, the factors that causegeometric asymmetry are the being of angle of attack or side slip angle, non-circular cross-section of the nose and asymmetric surface ablation [1].

[*] Ph.D. Candidate, Department of Mechanic & Aerospace, IHU University, Tehra, I. R. Iran, mme_engine56@yahoo.com

[†] Corresponding Author, Associate Professor, Department of Mechanic & Aerospace, IHU University, Tehran, I. R. Iran, mdostdar@ihu.ac.ir

One of the requirements to design the hypersonic vehicles, are access to accurate estimate of the aero-heating. For this reason, the research trend in this field is under development.
By using the newton's theory [1], the elementary commercial code to estimate the aero-heating has been created by "Dejarnet and Hamilton (1973) [2]. The viscous shock layer equations have been presented by "Carrel and Larry (1975) [3]. After identification of VSL[2] and SVBL[3] of FNS[4] for polar blunt body, the viscous shock layer equations for the non-ablative noses have been solved by "Miner and Lewis (1975) [4], this solution has been modified by "Brykina and Scott (1998) for geometric asymmetry caused by the angle of attack, [5]. After identification of the effects of chemical reactions and surface ablation, the" Dexygen researcher team (2012) has been used the created UDF[5] code based on the fluent software in order to estimate the more accurately of aero-heating [6]. This research has been modified by "Chen and Milos (2013) for any ablative material [7]. The numerical modeling of the flow field around hypersonic noses to compute the effects of air ionization/dissociation, equilibrium thermodynamics, and chemical imbalances assuming with fully implicit finite volume method has been conducted by "Benjamin et al. (2014) [8]. This modeling has been conducted by Doustdar et al. (2016, 2017) to create the CTCA Code by space marching method with fully implicit finite difference method during flight trajectory. The results of it have been validated for aero-heating modeling on the ablative noses, investigation of wall catalytic effects on the aero-heating of hypersonic ablative noses, simulation of temperature distribution for hypersonic ablative noses, and numerical simulation of radiance effects on the aerodynamic heating of ablative noses [9-12].

Therefore in this paper an accurate estimation of aero-heating is presented by using the numerical space marching solvers such as VSL and SVBL methods for the ablative and asymmetrical 3D noses of supersonic and hypersonic vehicles during flight trajectory. So, in this research, the effects of causer factors of geometric asymmetry on the aero-heating and surface temperature are modeled. The selection of method to solve the flow field and modeling the effects of geometric asymmetry on the aero-eating and surface temperature will be done, so that:

- The results accuracy of aero-heating as compare with the similar studies should not be changed.
- The surface ablation and non-equilibrium chemical reactions effects on the aero-heating should be considered.
- The time of solution during flight trajectory should be reduced, significantly.

2 Solution methods

Along with promote and develop the aerodynamic knowledge, different methods such as analytical and numerical have been created for an estimation of aero-heating. The combination of viscous shock layer method at nose surface and similarity solution of viscous boundary layer at stagnation point is the most optimal method in standpoint of accuracy and less solution time among the different numerical solution methods. In this method, the VSL method is used to solve the flow field around the blunt body, and the SVBL method is used to solve the flow field at stagnation points [13, 14]. The requirements to solve the equations of VSL-SVBL are:

[1] AEROHEAT Software
[2] Viscous shock layer
[3] Similarity of viscous boundary layer
[4] Fully Navier Stocks
[5] User Defined Function

- The FD[1] algorithm should be used.
- At shock layer, the structural mesh should be used.
- Because all terms up to Reynolds square order from FNS to create the VSL and SVBL, are eliminated, the curvature coordinate should be used in order to solve these equations.
- The curvature mesh grid should be converted into the hexagonal mesh grid[2] by mapping functions.

In according to mentioned preamble, to accurate and fast estimation of the aero-heating during flight trajectory, the combination of the VSL-SVBL methods is used. In this condition, the UDF based on the fluent solvers cannot be used. Therefore, the creating of solver is complicated but the solution time will be reduced, significantly.

In according to mentioned requirements, the following algorithms, to create the solver for asymmetry flow field around the ablative noses of hypersonic vehicles, should be used:

- The implicit Davis algorithm to solve the parabolic flow equations on the nose body.
- An algorithm to solve the flow equations at stagnation points.
- The ablative Park algorithm to combustion modeling.
- The non-equilibrium chemical reactions algorithm for modeling the dissociation/ionization of air at shock layer.
- The curve fitting algorithm to calculate the transfer and thermodynamic properties of species at shock layer by using the molecular theories results.
- The Wile algorithm to calculate the transfer and thermodynamic properties of gas mixture at shock layer.
- The Brykina and Scott theory for modeling the geometric asymmetry effects

3 Assumptions

- The flow equations at nose body are parabolic PDEs[3] and the boundary layer at stagnation point is thin.
- Due to dissociation/ionization of air, the non-equilibrium chemical reactions exist at shock layer and the species are diffused into the shock layer.
- The non-equilibrium chemical reactions exist on the ablator surface and the species are diffused into the shock layer.
- The thermodynamic and transfer properties of species are function of the elements temperature, and to calculate of them, the curve fitting based on the Polar Molecular theories and spectrographic test results is used.
- To consider the effects of surface ablation, the validated Park model is utilized.
- For modeling the geometric asymmetry effects, the Brykina and Scott theory is utilized.
- To calculate the source terms of species, the transient mass action law is utilized.
- To consider the effects of the natural convection heat transfer of air in nose inside, the effective equivalence thermal conductivity is calculated.
- At hypersonic flow (nose body), the eddies due to flow turbulence are 2D[4] and they are modeled by the Baldwin-Lomax model.
- The gaseous mixture of shock layer is a transparent body because one of the requirements to utilize the space marching algorithm is preventing of data propagation from downstream into upstream.

[1] Finite Difference
[2] Computational Domain
[3] Partial Differential Equations
[4] Two Dimensional

4 Governing Equations

4.1 Geometry and Mesh Grid [4, 5]

The blunt radius, variations of body surface, body angle (θ) and curvature (χ) are defined at any meridional plane of the nose in direction of z axis (see Figure (1)). The required geometric parameters are derived by utilizing the Lagrange interpolation polynomial equations [5].

$$F(X)=\sum_{K=1}^{3} f_K L_K(x) \quad L_K(x)=\prod_{m=1,m\neq K}^{3}\frac{x-x_m}{x_K-x_m} \tag{1}$$

$$\chi=\frac{\left|\frac{d^2r}{dz^2}\right|}{(1+(\frac{dr}{dz})^2)^{\frac{3}{2}}}=\sqrt{(\frac{d^2r}{ds^2})^2+\frac{d^2z}{ds^2})^2} \quad s=\sqrt{z^2+r^2} \quad \alpha=\theta+tg^{-1}(\frac{\partial y_{sh}}{1+\chi y_{sh}}) \tag{2}$$

In the Equation (2), θ, y_{sh} are body angle and shock layer thickness, respectively. For mesh gird in the curvature coordinates:

$$dy=\begin{cases}\frac{1}{N-1} & P_K=1\\ \frac{P_K-1}{P_K{}^{N-1}} & P_K>1\end{cases} \quad P_K: grid\ \ scale \quad dn_{i+1}=P_K\times dn_i \quad xn_{i+1}=xn_i+dn_i \quad xn_1=0 \tag{3}$$

In according the following procedure, the Brykina and Scott theory is used in order to create an EAB[1].

a. Calculate the mean curvature of an EAB and main body

$$H_s=\frac{\chi+r^{-1}}{2} \quad H=\frac{f_{xx}(1+f_y{}^2)+f_{yy}(1+f_x{}^2)-2f_{xy}f_xf_y}{2(1+f_x{}^2+f_y{}^2)^{1.5}}$$
$$f_x=\frac{\partial f}{\partial x} \quad f_y=\frac{\partial f}{\partial y} \quad f_{xx}=\frac{\partial^2 f}{\partial x^2} \quad f_{yy}=\frac{\partial^2 f}{\partial y^2} \quad f_{xy}=\frac{\partial^2 f}{\partial x\partial y} \tag{4}$$

b. at stagnation point $\theta=\pi/2, z_n=s_n=0$. To calculate x_n, y_n, z_n at the other points:

$$x_n=(z-z_0)\sin\alpha+(x-x_0)\cos\alpha \quad z_n=(z-z_0)\sin\alpha-(x-x_0)\cos\alpha \quad y_n=y$$
$$f_{x_0}=tg\alpha, z_0=f(x_0\quad 0), y=x_n tg\varphi=\left[(z-z_0)\sin\alpha+(x-x_0)\cos\alpha\right]tg\varphi \quad \sin\theta=\frac{fx\sin\alpha+\cos\alpha}{\sqrt{1+f_x{}^2+f_y{}^2}} \tag{5}$$

c. Calculate r_n, s at the stagnation point and other points of an EAB:

[1] Equivalent axisymmetric body

$$\frac{dr_n}{dx}=\begin{bmatrix}\begin{bmatrix}\frac{dr_n}{dy}=1 & \varphi=\frac{\pi}{2}\\ \frac{dr_n}{dy}=\frac{f_{xx0}+d_0{}^2 f_{yy0}}{\sqrt{f_{xx0}{}^2\cos\alpha^2+d_0{}^2 f_{yy0}{}^2}} & \varphi\neq\frac{\pi}{2}\end{bmatrix} & \theta=\frac{\pi}{2}\\ tg\alpha\left[\left(f_x+df_y\right)\cos\alpha-\sin\alpha\right] & \theta\neq\frac{\pi}{2}\end{bmatrix}$$

$$\frac{ds}{dx}=\begin{bmatrix}\frac{ds}{dy}=\frac{dr_n}{dx}=\frac{dr_n}{dy} & \theta=\frac{\pi}{2}\\ \frac{1}{\cos\alpha}\left[\left(f_x+df_y\right)\cos\alpha-\sin\alpha\right] & \theta\neq\frac{\pi}{2}\end{bmatrix} \tag{6}$$

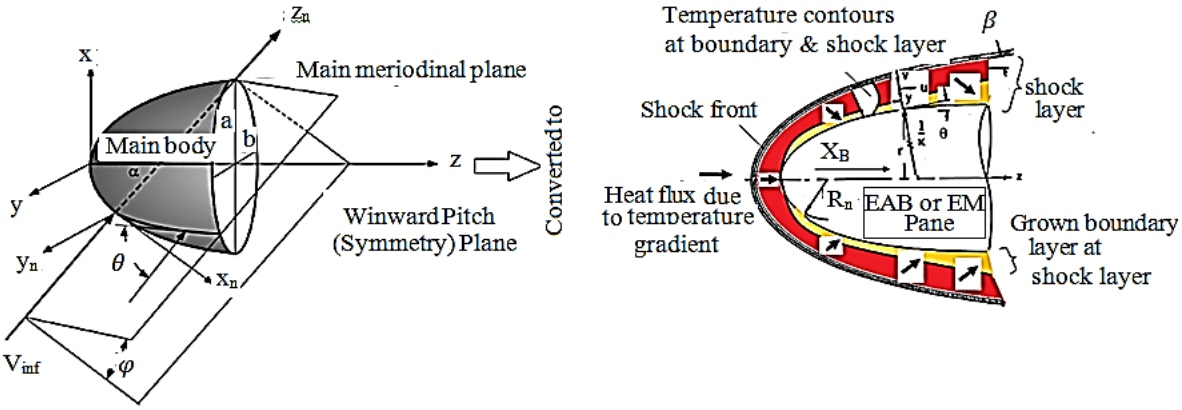

Figure 1 Main and EAB bodies [1, 6]

d. Calculate the curvature of an EAB:

$$\chi=\begin{bmatrix}\begin{bmatrix}\frac{a_2a_1+a_2f_yb_2}{b_3\left[\left(f_x+df_y\right)\cos\alpha-\sin\alpha\right]} & \varphi\neq\frac{\pi}{2}\\ \frac{f_{xy}a_1+f_{yy}f_yb_2}{f_y\cos\alpha b_3} & \varphi=\frac{\pi}{2}\end{bmatrix} & \theta=\frac{\pi}{2}\\ \begin{bmatrix}\frac{c_1{}^2\cos\alpha+d_0c_2f_{yy_0}b_{2_0}}{c_3(f_{xx_0}+2d_0f_{xy_0}+d_0{}^2f_{yy_0})} & \varphi\neq\frac{\pi}{2}\\ \frac{f_{xy_0}{}^2\cos\alpha+f_{yy_0}b_{2_0}}{\cos\alpha f_{yy_0}c_3} & \varphi=\frac{\pi}{2}\end{bmatrix} & \theta\neq\frac{\pi}{2}\end{bmatrix} \qquad a_1=\left[f_x\cos\alpha-\sin\alpha\left(f_y{}^2+1\right)\right]$$

$$a_2=\left(f_{xx}+df_{yy}\right)\quad b_1=f_y{}^2+1\quad b_2=f_x\sin\alpha+\cos\alpha\quad b_3=(1+f_x{}^2+f_y{}^2)^{1.5}$$

$$c_1=f_{xx_0}+d_0f_{xy_0}\quad c_2=f_{xy_0}+d_0f_{yy_0}\quad c_3=\left(1+f_{x_0}{}^2\right)^{1.5}\quad d_0=\frac{b_{2_0}tg\varphi}{1-f_{y_0}\sin\alpha tg\varphi} \tag{7}$$

e. Calculate the ratio of mean curvatures for the main body to an EAB:

$$\frac{H}{H_s}=\begin{bmatrix}\dfrac{f_{xx}b_1+f_{yy}(1+f_x{}^2)-2f_{xx}f_xf_y}{(\chi+r_n^{-1}\cos\theta)b_3} & \theta\neq\dfrac{\pi}{2}\\ \dfrac{f_{xx0}b_{10}+f_{yy0}(1+f_{x0}{}^2)}{2\chi_0(1+f_{x0}{}^2)^{1.5}} & \theta=\dfrac{\pi}{2}\end{bmatrix} \tag{8}$$

d. The equations of the modified mesh due to the ablation with according to the chemical reaction rates at the ablative surface (Reactions 8 to 11):

$$V_{CS}=\frac{Rr_8+Rr_9+Rr_{10}+Rr_{11}}{\rho_C}\qquad X_{n_{cs}}=V_{CS}.dt \tag{9}$$

By using the magnitude of the surface recesses, the nose blunt radius and other required geometry variables are modified and with according to the new geometry variables, the mesh grid of gas mixture at shock layer is modified [15].

4.2 Flow Equations at Shock Layer [4]

The flow equations at shock layer are [4]:

a. Continuity Equation

$$\frac{\partial}{\partial s}\left((r+y\cos(\theta))^j\rho u\right)+\left(\frac{\partial}{\partial y}(1+\gamma y)(r+y\cos(\theta))^j\rho u\right)+\dot{M}_{cg} \tag{10}$$

b. S-Momentum Equation

$$\begin{aligned}&\frac{1}{1+\gamma y}\rho u\frac{\partial u}{\partial s}+\rho v\frac{\partial u}{\partial y}+\rho uv\frac{\gamma}{1+\gamma y}+\frac{1}{1+\gamma y}\frac{\partial P}{\partial s}=\Xi^2\frac{\partial}{\partial y}\left(\mu\left(\frac{\partial u}{\partial y}-\frac{\gamma u}{1+\gamma y}\right)\right)\\&+\Xi^2\left(\frac{\gamma}{1+\gamma y}+\frac{j\cos(\theta)}{r+y\cos(\theta)}\right)\left(\frac{\partial u}{\partial y}-\frac{\gamma u}{1+\gamma y}\right)\quad \Xi=\frac{1}{\mathrm{Re}}\end{aligned} \tag{11}$$

c. Y-Momentum Equation

$$\frac{\partial P}{\partial y}=\rho u^2\frac{\gamma}{1+\gamma y} \tag{12}$$

d. Energy Equation

$$\begin{aligned}&\frac{1}{1+\gamma y}\rho uC_p\frac{\partial T}{\partial s}+\rho vC_p\frac{\partial T}{\partial y}-\frac{1}{1+\gamma y}u\frac{\partial P}{\partial s}-v\frac{\partial P}{\partial y}=\Xi^2\frac{\partial}{\partial y}\left(k\frac{\partial T}{\partial y}\right)+\Xi^2\\&\left(\frac{\gamma}{1+\gamma y}+\frac{j\cos(\theta)}{r+y\cos(\theta)}\right)k\frac{\partial T}{\partial y}-\Xi^2\sum_{i=1}^{n_s}J_iC_{p_i}\frac{\partial T}{\partial y}+\Xi^2\mu\left(\frac{\partial u}{\partial y}-\frac{\gamma}{1+\gamma y}\right)^2-\sum_{i=1}^{n_s}h_i\dot{w}_i\end{aligned} \tag{13}$$

e. Species Conservation Equation

$$\begin{aligned}&\frac{1}{1+\gamma y}\rho u\frac{\partial C_i}{\partial s}+\rho v\frac{\partial C_i}{\partial y}=\dot{w}_i-\Xi^2\frac{\partial}{\partial y}(J_i)-\Xi^2\left(\frac{\gamma}{1+\gamma y}+\frac{j\cos(\theta)}{r+y\cos(\theta)}\right)J_i\\&J=\frac{-\mu}{\mathrm{Pr}}Le_i\frac{\partial C_i}{\partial y}\qquad C_i=\frac{\rho_i}{\rho}\end{aligned} \tag{14}$$

f. Equation of state

$$P=\frac{\rho RT}{\overline{M}C^*_{p_\infty}} \tag{15}$$

$\dot{M}_{cg}$ is injected gas into the shock layer due tom the surface ablation, J_i is diffusion mass flux term of species *i*. n_s is number of species in shock layer (due to dissociation, ionization of air and surface ablation). The magnitude of *J* is equal to zero for 2D and 1 for 3D symmetric bodies. $h_i, \dot{w}_i, C_{pi}$ are enthalpy, source term and specific heat at constant pressure of species *i*, respectively.

The shock-layer equations are transformed for the finite-difference solution procedure. The independent and dependent variables (except to the species concentrations) are normalized by their relevant local shock values.

When written in the transformed η, ζ coordinates, the s-momentum, energy, and continuity equations can be expressed in the following standard form for the parabolic PDEs (except of stagnation points):

$$\frac{\partial^2 W}{\partial \eta^2} + A_1 \frac{\partial W}{\partial \eta} + A_2 W + A_3 + A_4 \frac{\partial W}{\partial \zeta} \tag{16}$$

The details of A_1, A_2, A_3, A_4 equations have been presented in [4].

4.3 Source Terms Equations [4, 18]

In dissociation and ionization process, air during 7 chemical reactions is converted into the 6-species (*i=1…6*), such as atom and molecule of oxygen (O, O_2), atom and molecule of nitrogen (N, N_2), nitrogen oxide molecule (NO), nitrogen oxide ion (NO^+), and electrons (e^-) [8, 16].

To calculate the concentration of species due to chemical reactions of air, non equilibrium chemical assumption is used. Therefore, the forward and backward chemical reaction rate constants are not equal:

$$k_{fr} = T_k^{CR2} \exp\left(\ln(CR_{0R}) - \frac{CR_1}{T_k}\right), k_{br} = T_k^{DR2} \exp\left(\ln(CR_{0B}) - \frac{DR_1}{T_k}\right) \tag{17}$$

$CR_{0R}, CR_1, CR_2, DR_{0R}, DR_1, DR_2$ are constants related to any forward and backward chemical reactions of air. For the mass concentration of the mentioned species:

$$\gamma_j = \frac{C_j}{M_j} \quad C_j = \frac{\rho_j}{\rho} \quad \gamma_j = \frac{C_j}{M_j} \quad j = 1...6 \quad C_j = \frac{\rho_j}{\rho} \tag{18}$$

In order to calculate the concentration of catalytic third body, the third body efficiency relative to argon z_{j-n_S} should be calculated [17].

$$\begin{array}{lll} O_2 \xleftrightarrow[M1]{} 2O & N_2 \xleftrightarrow[M2]{} 2N & NO \xleftrightarrow[M3]{} N + O \quad N_2 + N \xleftrightarrow[4]{} N + N + N \\ NO + O \xleftrightarrow[5]{} N + O_2 & N_2 + O \xleftrightarrow[6]{} NO + N & N + O \xleftrightarrow[EL]{} NO^+ + e^- \end{array} \tag{19}$$

For source terms of species at flow field:

$$\frac{\dot{w}_i}{\rho} = w_i^0 + w_i^1 C_i \quad w_i^0 = \mu_i \sum_{r=1}^{n_r} \left(\Gamma_{ri}^+ L_{fr} + \Gamma_{ri}^- L_{br} \right) \quad w_i^1 = \sum_{r=1}^{n_r} \left(\Gamma_{ri}^+ \frac{L_{br}}{\gamma_i} + \Gamma_{ri}^- \frac{L_{fr}}{\gamma_i} \right) \tag{20}$$

$$\Gamma_{ri}^+ = \begin{cases} \beta_{ri} - \alpha_{ri} & if.\beta_{ri} - \alpha_{ri} \geq 0 \\ 0 & if.\beta_{ri} - \alpha_{ri} < 0 \end{cases} \quad \Gamma_{ri}^- = \begin{cases} -(\beta_{ri} - \alpha_{ri}) & if.\beta_{ri} - \alpha_{ri} < 0 \\ 0 & if.\beta_{ri} - \alpha_{ri} \geq 0 \end{cases}$$

$$L_{fr} = K_{fr} \bar{\rho}^{\alpha r} \prod_{j=1}^{10} \gamma_j^{\alpha r_j} \qquad L_{br} = K_{br} \bar{\rho}^{\beta r} \prod_{j=1}^{10} \gamma_j^{\beta r_j} \tag{21}$$

Where αr_j, βr_j are stoichiometric coefficients of forward and backward chemical reactions of air.

$$\frac{\partial}{\partial T_k}(\frac{\dot{w}_i}{\rho}) = \frac{M_i}{T_k}\sum_{r=1}^{nr}(\beta_{ri}-\alpha_{ri})\left(\left(C2_r+\frac{C1_r}{T_k}-\alpha r\right)L_{fr}-\left(D2_r+\frac{D1_r}{T_k}-\beta r\right)L_{br}\right) \tag{22}$$

For source terms $\dot{w}_i$ of species *i* due to dissociation and ionization of air at *(k+1)th* iteration[8, 13, 14]:

$$(\frac{\dot{w}_i}{\rho})_{k+1} = (\frac{\dot{w}_i}{\rho})_k + \left(\frac{\partial}{\partial T_k}(\frac{\dot{w}_i}{\rho})_k (T_{k+1}-T_k)\right) \tag{23}$$

The rate of surface recess due to ablation chemical reactions is calculated by using the Park model with equilibrium thermodynamic assumption. The accomplished chemical reactions at char section are as follows:

- Char Oxidation: $C(s)+O \xleftrightarrow[8]{} CO$
- Char Oxidation: $C(s)+1/2O_2 \xleftrightarrow[9]{} CO$
- Char Nitration: $C(s)+2N \xleftrightarrow[10]{} CN+N$
- Char Sublimation: $3C(s) \xleftrightarrow[11]{} C_3$

For charring ablators in pyrolysis zone, the hydrogen is pyrolyzed. This gas is reacted with char and CH_2 will be produced. CH_2 is dissociated and the hydrogen gas is produced. The productions of char and non-char surface ablations are as follows [18, 19]:

$$\begin{array}{ll} CO, CN, C_3, C_2, C, CH_2, H_2, H & \textit{Char ablators} \\ CO, CN, C_3, C_2, C & \textit{non Char ablators} \end{array} \tag{24}$$

For the rate of reactions at ablator surface:

$$Rr_8 = \rho C_1\sqrt{\frac{\sigma T_W}{2\pi C_1 M_1}}\frac{\beta_1 M_{11}}{M_1} \qquad Rr_9 = \rho C_2\sqrt{\frac{\sigma T_W}{2\pi C_2 M_2}}\beta_1\frac{M_{11}}{M_2}$$

$$Rr_{10} = \rho C_4\sqrt{\frac{\sigma T_W}{2\pi C_4 M_4}}\frac{\beta_1 M_{11}}{M_4} \qquad Rr_{11} = \rho(C_{9E}-C_9)\sqrt{\frac{\sigma T_W \beta_9^{\,2}}{2\pi C_9 M_9}}$$

$$\beta_1 = 0.63\exp(\frac{-1160}{T_W}),\ \beta_2 = 0.5,\ \beta_4 = 0.3,\ \beta_2 = 1,\ C_{9E} = \frac{5.19E15\exp(\frac{90845}{T_W})}{p} \tag{25}$$

$$V_W = \frac{Rr_8 + Rr_9 + Rr_{10} + Rr_{11}}{\rho}$$

Where *P* is the gas pressure entered into the shock layer, and V_{CS}, V_W, ρ_C are surface recessions, gas blowing velocity to shock layer from char zone and carbon density, respectively. For source terms of surface ablation species with according the Park model:

$$\dot{w}_1 = -Rr_8\frac{M_1}{M_{11}} \quad \dot{w}_2 = -Rr_9\frac{M_2}{M_{11}} \quad \dot{w}_3 = -Rr_{10}\frac{M_4}{M_{11}} \quad \dot{w}_4 = -Rr_{11} \quad \dot{w}_5 = 0 \quad \dot{w}_6 = 0$$

$$\dot{w}_7 = Rr_8\frac{\dot{M}_7}{M_{11}} + Rr_9\frac{M_7}{M_{11}} \quad \dot{w}_8 = -Rr_{10}\frac{M_8}{M_{11}} \quad \dot{w}_9 = 0, \dot{w}_{10} = 0, \quad \dot{w}_{11} = 0 \tag{26}$$

The species concentration on the surface of non-char ablator is calculated by using the equation 27 and iteration of its loop.

$$C_{i,new} = C_{i,old} + \frac{\dot{w}_i\, dt}{(dz)\rho} \quad \max(\delta i) = \max(\frac{C_{i,new} - C_{i,old}}{C_{i,old}}) \quad C_{i,old} = C_{i,new} \tag{27}$$

$$if\ \max(\delta i) > 0.001 \quad return$$

The mentioned loop is repeated for all of the species due to ablation except that:

$$\dot{w}_{12} = 0 \quad \dot{w}_{14} = 0 \quad \dot{w}_{13} = \rho V_W (1 - \frac{\rho_{CH}}{\rho_V}) \quad Rr_{gas} = \rho V_W (1 - \frac{\rho_{CH}}{\rho_V}) \quad V_{cs} = \frac{Rr_{gas}}{\rho_V - \rho_{CH}} \tag{28}$$

Where ρ_V, ρ_{CH} are density of char and virgin material, respectively.
The details of Source terms equations have been presented in [10].

4.4 Thermodynamic, Transfer Properties [20]

The thermal conductivity and dynamic viscosity of species *i*, are calculated by the curve fitting of Leonard Jones and Stock Mires theories, and the diffusion model is limited to the binary diffusion (two gas spectrum according to molecular weight). The binary diffusion coefficients specified by the Lewis number so the Thermal conductivity and dynamic viscosity of mixture, are calculated by using the semi-empirical equations of Wilke [20].

The specific heat at constant pressure and enthalpy of species *i*, are calculated by Lagrange interpolation of spectrograph test results. For enthalpy and frozen specific heat of mixture:

$$C_{p,\,frozen} = \sum_{i=1}^{14} C_i C_{p_i} \qquad h = \sum_{i=1}^{14} C_i h_i \tag{29}$$

4.5 Radiation Heat Transfer [12]

The radiation heat transfer is calculated by using the experimental tables of absorption coefficients of high temperature air as a function of frequency. In these calculations, it's assumed that the gaseous mixture of shock layer is a transparent body because one of the requirements to utilize the space marching algorithm is preventing of data propagation from downstream to upstream. This requirement is violated by using the absorption-radiant assumption for the gaseous mixture of shock layer.

$$q_R = 2\pi J \delta_{sh} \quad ER = \frac{2q_R}{\delta_{sh}} \quad J = \int_0^\infty k_\nu \frac{2h\nu^3}{c^2(\exp(\frac{h\nu}{KT}) - 1)} d\nu \tag{30}$$

Where q_R, δ_{sh} are the radiation heating and shock layer thickness, respectively [20, 21].
The details of Radiation Heat Transfer Equations have been presented in [12].

4.6 Aero-heating and surface transfer equations [9]

The rate of the heat transfer and surface friction can be calculated by using the surface friction coefficient and Stanton number [4, 20]:

$$C_f = \frac{2\overset{*}{\tau}_W}{\overset{*}{\rho}_\infty \overset{*}{U}_\infty^2} \quad \overset{*}{\tau}_W = \left(\overset{*}{\mu} \frac{\partial \overset{*}{u}}{\partial \overset{*}{y}} \right)_W \tag{31}$$

The surface friction coefficient as a function of the dimensionless variables and Stanton number:

$$St = \frac{\overset{*}{q}_W}{\overset{*}{\rho}_\infty \overset{*}{U}_\infty \left(\overset{*}{H}_\infty - \overset{*}{H}_W \right)} \quad \overset{*}{q}_W = -\left(\overset{*}{k} \frac{\partial \overset{*}{T}}{\partial \overset{*}{y}} - \sum_{i=1}^{14} \overset{*}{h}_i \overset{*}{J}_i \right)_W + \overset{*}{q}_R \tag{32}$$

The details of Aero-heating and surface transfer Equations have been presented in [9].

4.7 Turbulent Modeling Equations [22]

The experimental results show that the size of eddies due to turbulent at very high velocities is small and therefore, a 2-D simulation can be performed with the Baldwin-Lomax turbulent model. In this model, the effects of turbulent on the FNS are accounted by adding proper terms to the thermal conductivity coefficients and dynamic viscosity [22, 23]:

$$\mu_{new} = \mu_{old} + \mu_T \quad k_{new} = k_{old} + k_T \tag{33}$$

The details of Turbulent Modeling Equations have been presented in [22].

5 Boundary Conditions

5.1 Velocity boundary conditions [4]

At the shock, the tangential and normal velocity components on shock are not the same as the tangential and normal velocity components on body surface. The tangential and normal velocity components on shock are denoted by $\hat{u}_{sh}, \hat{v}_{sh}$ and the tangential and normal velocity components on body surface are denoted as u_{sh}, v_{sh}. The transformation of relating the two sets of shock velocity components is as follows [4]:

$$u_{sh} = \hat{u}_{sh} \sin(\beta' + \beta) + \hat{v}_{sh} \cos(\beta' + \beta) \quad v_{sh} = -\hat{u}_{sh} \cos(\beta' + \beta) + \hat{v}_{sh} \sin(\beta' + \beta) \quad \beta' = \frac{\pi}{2} - \theta \tag{34}$$

For the shocks of finite thickness called SS[1], the shock properties are given by the modified Rankin - Huguenot relations.

$$\hat{v}_{sh} \rho_{sh} = \sin(\beta) \quad \Xi^2 \mu_{sh} \left(\frac{\partial \hat{u}}{\partial y} \right)_{sh} = \sin(\beta)\cos(\beta) \quad P_{sh} - \sin(\beta) \hat{v}_{sh} = \frac{P\infty}{\rho_\infty {U_\infty}^2} + \sin^2(\beta) \tag{35}$$

For the NSS[2], the Rankin - Huguenot relations are used to change the equation 35: $\hat{u}_{sh} = \cos(\beta)$

5.2 Temperature boundary conditions

The temperature of the boundary of downstream is calculated by using the extrapolation of shock layer grid and its magnitude on the wall is different for the cases such as: constant temperature wall, adiabatic wall and no adiabatic wall. In this research, it is assumed that the wall is no adiabatic and the wall temperature is determined simultaneously by solving the heat transfer PDE inside the body, surface, and ablator zones [4, 19].

$$\Xi^2 k_{sh} \left(\frac{\partial T}{\partial y} \right)_{sh} + \sin(\beta) \sum_{i=1}^{14} C_{i_\infty} h_{i_{sh}} - \frac{\sin(\beta)}{2}, \left(\left(\hat{u}_{sh} - \cos(\beta) \right)^2 + \sin^2(\beta) - \hat{v}_{sh} \right) = \sin(\beta) \sum_{i=1}^{14} C_{i_\infty} h_{i_\infty} \tag{36}$$

[1] shock slip
[2] no shock slip

The Rankin - Huguenot relation for NSS:

$$\sum_{i=1}^{14} C_{i_\infty} h_{i_{sh}} - \frac{\left(\hat{u}_{sh} - \cos(\beta)\right)^2}{2} + \frac{\left(-\hat{v}_{sh} + \sin^2(\beta)\right)}{2} = \sum_{i=1}^{14} C_{i_\infty} h_{i_\infty} \tag{37}$$

5.3 Boundary conditions of Species concentration

For a NCW[1], the boundary conditions of species are as: $\partial C_i / \partial \eta = 0$

The ECW[2] conditions are specified by $C_i = C_{i_{eq}} T_W$

In this research, the ECW condition is approximated by a FCW[3] condition at initial time step. At initial time step, the species concentrations due to the surface ablation are zero, and in the next time steps, the species concentrations are modified by using the Park model [4, 19].

$$C_O = 0 \quad C_{O_2} = 0.23456 \quad C_{NO} = 0 \quad C_N = 0 \quad C_{NO^+} = 0 \quad C_{N_2} = 0.76544 \tag{38}$$

The SS and NSS shock properties are given by the modified Rankin - Huguenot relations.

$$\Xi^2 \frac{\mu_{sh}}{\mathrm{Pr}_{sh}} Le_i \frac{\partial C_{i_{sh}}}{\partial y} + \sin(\beta) C_{i_{sh}} = \sin(\beta) C_{i_\infty} \quad for\ SS \qquad C_{i_{sh}} = C_{i_\infty} \quad for\ NSS \tag{39}$$

5.4 Shock conditions

The shock conditions for the dependent variables (at η = 1) are as follow [4]:

$$\bar{u} = \bar{v} = \bar{\rho} = \bar{P} = \bar{T} = 1 \qquad C_{i_{sh}} = C_{i_\infty} \tag{40}$$

The details of Boundary Condition Equations have been presented in [11].

6 Solver Algorithms

6.1 Davis algorithm

Taylor series expressions are used to relate the partial derivatives to the function values at the finite-difference grid points with the finite-difference grid [24].

6.2 Y-momentum solver algorithm

The normal momentum equation is rewritten so that $\partial \bar{P} / \partial \eta$ may be evaluated directly. The pressure derivative with respect to η is calculated with the y-momentum equation.

With $\bar{P}$ at the shock known $\bar{P}_{sh} = 1$, the integration by the trapezoidal rule from the shock inward gives the solution of the normal momentum equation [25].

6.3 Continuity solver algorithm

By integration, the trapezoidal rule from the shock inward gives the solution of continuity equation. Two parameters are calculated, i.e. normal velocity profiles *(v)* and shock layer thickness y_{sh} [25].

---

[1] non-catalytic surface
[2] equilibrium catalytic wall
[3] fully catalytic wall

6.4 Surface ablation algorithm

In this algorithm, dependent on the type of ablator (char or non-char), the chemical reactions are defined by using the Park model, and the rate of these reactions is calculated by using the equilibrium thermodynamic assumption. Then, the source terms and species concentration due to surface ablation are calculated. The energy equation is derived at ablator surface. After definition of the radiation effluence coefficient of the gaseous mixture attached to the wall and the discretion of differential terms, the energy equation at ablator surface is solved in order to calculate the wall temperature by using the Newton-Raphson method [6].

$$(-k_{xw}\zeta_x - k_y\zeta_y)\frac{\partial T}{\partial \zeta} + (-k_x\eta_x - k_y\eta_y)\frac{\partial T}{\partial \eta} - k_y\left(\frac{\partial T}{\partial z}\right)_{gas,W} - \sum_{i=1}^{n_{s_1}} h_i T_W \dot{w}_i + \alpha \overset{*}{q}_r - \sigma\varepsilon T_W{}^4 = 0 \qquad (41)$$

The details of Solver Algorithms and main Flowchart of CTCA Code have been presented in [11].

7 Convergence Criteria

The convergence criteria are calculated by using this equation (*n* is number of iteration).

$$\varepsilon = \max\left(\begin{array}{l}\max\left(\left|\frac{1-T_n}{T_{n-1}}\right|\right), \max\left(\left|\frac{1-u_n}{u_{n-1}}\right|\right), \max\left(\left|\frac{1-v_n}{v_{n-1}}\right|\right) \\ , \max\left(\left|\frac{1-C_{i,n}}{C_{i,n-1}}\right|\right)\end{array}\right) < 0.01 \quad i = 1...14 \qquad (42)$$

8 Results

Figure (2) shows the calculated aerodynamic-heating magnitudes for a 2-D Parabolic curvature for these geometry characteristics, blunt radius and flight conditions [6]:

$$k = (\frac{big..dia}{small..dia})^2 = (\frac{a}{b})^2 = 0.25, V = 6\frac{km}{s}, h = 95km, Bend...Radii(R_n) = 0.4m, \alpha = 0^0$$

In the figures (3-5), The Induced Aero-heating and Surface Temperature Ratio of a non ablative typical nose at zero and 180 degree of meriodinal plane are showed. In according with figure (1), for the geometry characteristics, blunt radius and flight conditions:

$$k = (\frac{big\ dia}{small\ dia})^2 = (\frac{a}{b})^2 = 0.25 \quad V = 6\frac{km}{s} \quad h = 95km \quad Bend\ \ Raduis(R_n) = 0.4m \quad \alpha = 15^0, 30^0, 45^0$$

In these figures, the results are compared with written UDF code predicated of fluent software [6]. At all of these figures, the x' parameter is:

$$x' = -\left(\frac{\left(x^2 - tg^2\alpha\right)\sin(\alpha)}{2} + \left(x - tg(\alpha)\right)\cos(\alpha)\right) \qquad (43)$$

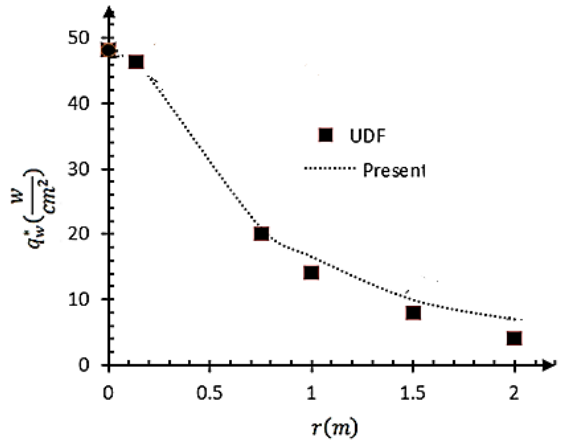

Figure 2 Induced Aero-heating for a 2-D Parabolic curvature at zero angle of attack

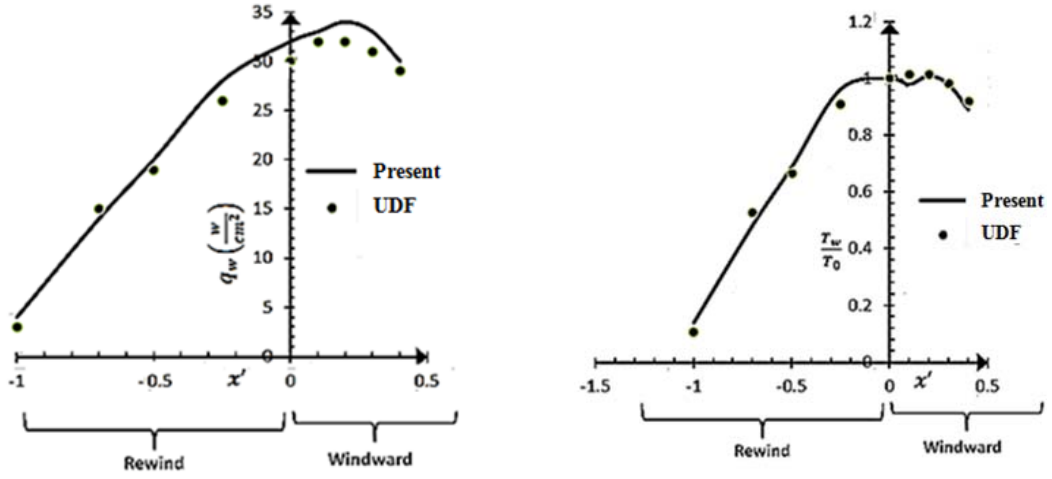

(a) Induced Aero-heating (b) Surface Temperature Ratio

Figure 3 Induced Aero-heating and Surface Temperature Ratio of a non-ablative typical nose at $\alpha = 15^0$

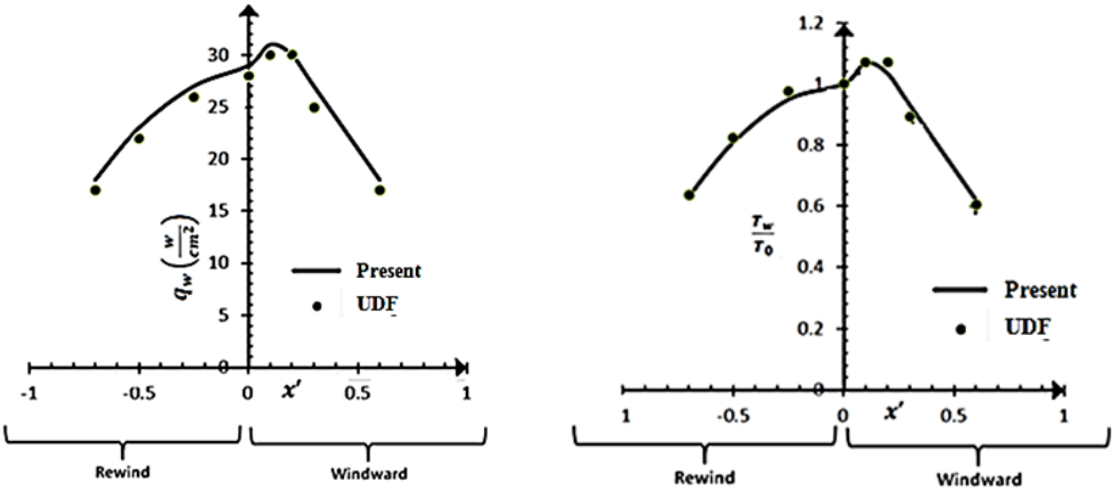

(a) Induced Aero-heating (b) Surface Temperature Ratio

Figure 4 Induced Aero-heating and Surface Temperature Ratio of a non-ablative typical nose at $\alpha = 30^0$

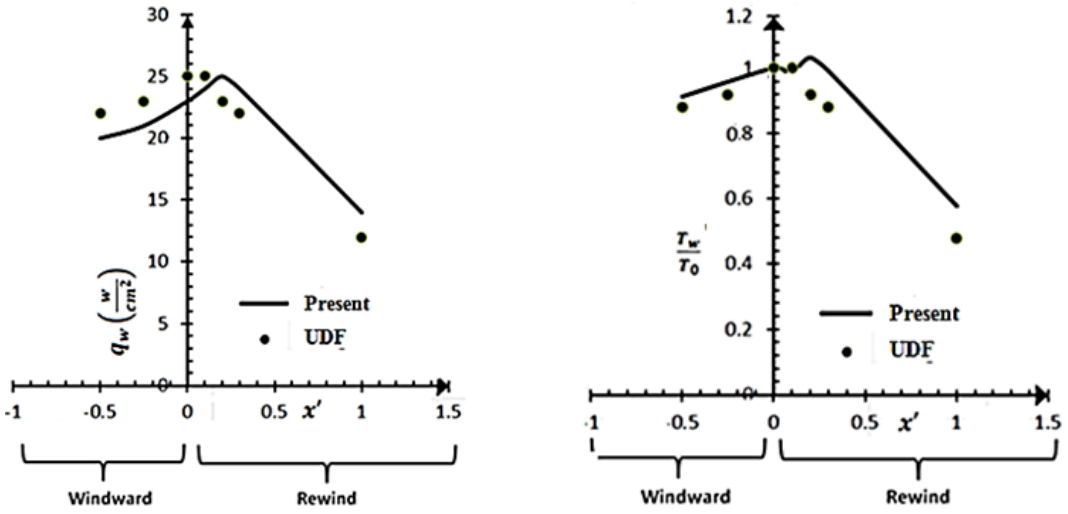

(a) Induced Aero-heating (b) Surface Temperature Ratio

Figure 5 Induced Aero-heating and Surface Temperature Ratio of a non-ablative typical nose at $\alpha = 45^0$

The results of VSL and SVBL to calculate the aero-heating show that, they matches with the FV solution results of FNS with the relative error less than 6% & 8% for an Aero-heating and surface temperature.

Figure (6) shows the calculated surface recess due to the ablation at stagnation point of it (This condition was kept for 45 seconds), and the result is compared with results of Ref [26]. In these comparisons, the flight condition and the data of geometry are as follow:

$$k = 0.25 \quad V = 6\frac{km}{s} \quad h = 95km \quad R_n = 0.4m$$

Figure (7) shows the variation of aero-heating magnitude (results of this research) of typical nose installed on vehicles in according to the curvature distance (s) and time (t), which the maximum Mach number and flight height are 6 and 60km respectively.

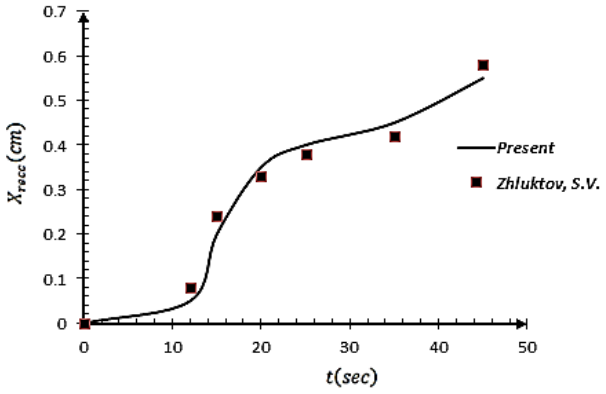

Figure 6 Comparison of calculated recess at stagnation point for a typical carbon-phenolic composite nose with Ref [26]

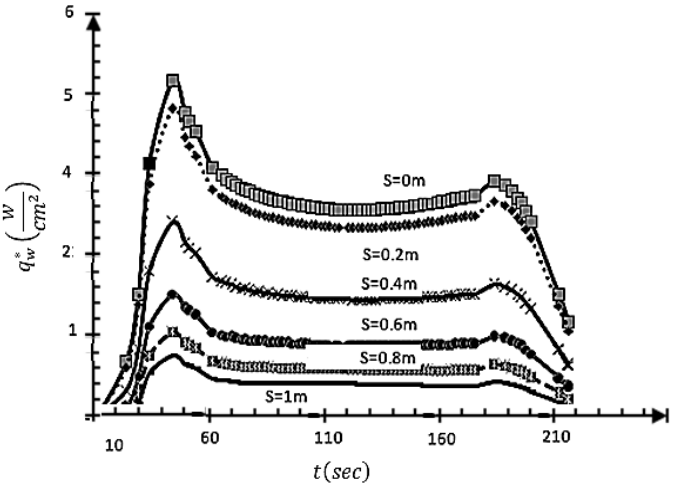

Figure 7 Variation of aero-heating magnitude of the typical nose in according to the *s* and *t*

In the figure (6), the surface recess due to ablation is calculating with the relative error less than 11%. In the figure (7), the rational trend of aero-heating variation has been showed with flight time of trajectory.

9 Conclusion

In this paper, the combined of VSL-SVBL methods, Park ablation, Baldwin-Lomax turbulent models is presented. This numerical combine methodology is used here to calculate the aero-heating for ablative noses during flight trajectory.

- The simulation results to calculate the aero-heating and surface temperature of the axisymmetric ablative noses during flight trajectory with the UDF method and FV solvers is not good because the solution time of it is very high.
- This combined method is created based on the FD method.
- The advantages of this method, is reducing the time to solve of the PDEs and computational memory, significantly.
- The mentioned advantages will be significant for the unsteady analysis of ablative noses at high and medium range of vehicles specifically, during flight trajectory.
- The time of solution for a typical axisymmetric nose during flight trajectory was reduced by 85% as compare to the UDF solver based on the fluent software.
- The results of this research are validated by the other researches.
- The relative error of the aero-heating, surface temperature and surface ablation results is less than 6,8,11 per cent in, respectively.

Acknowledgments

The research described in this paper was supported by the Mechanic and Aerospace Colleague of Imam Hussein University of Iran.

References

[1] Anderson, J., "*Hypersonic and High Temperature Gas Dynamics*", Second Edittion, McGraw-Hill, New York: ISBN:978-964-2751-04-4. pp. 325-346, (1989).

[2] Dejarnet, F.R., and Hamilton, H.H., "Inviscid Surface Streamlines and Heat Transfer on Shuttle-type Configuration", Journal of Spacecraft, Vol. 10, No. 5, pp. 314-321, (1973) .

[3] Carrel, B., Larry, W., and Thomas, J., "A Coupled Computer Code for the Transient Thermal Response and Ablation of Non-charring Heat Shields and Nose Tips", National Aeronautics and Space Administration, Vol. 4, No. 2, pp. 21-32, (1970) .

[4] Miner, E.W., "Computer User's Guide for a Chemically Reacting Viscous Shock Layer Code", Vol. 8, No. 6, NASA CR-2551, pp. 24-32, (1975).

[5] Brykina, C., and Scott, D., "An Approximate Axisymmetric Viscous Shock Layer Aeroheating Method for Three-dimensional Bodies", AIAA NASA, TM198-207890, Vol. 11, No. 5, pp. 14-22, (1998).

[6] Dexygen1.6.1, G.R., "Ablation Modeling of Nose Section with UDF Linkage to Fluent Software", Journal of Thermophysicsand Heat Transfer, Vol. 14, No. 3, pp. 32-41, (2012).

[7] Chen, Y.K., and Melos, F.S., "Finite-rate Ablation Boundary Conditions for Carbon-phenolic Heat-shield", NASA Ames Research Canter, and Moffett Field, CA 94035-1000, Vol. 7, No. 3, pp. 41-54, (2013).

[8] Benjamin, S., Roy, H., Paul, H.S., Baumanb, T., and Oliver, T. A., "Modeling Hypersonic Entry with the Fully-implicit Navier–Stokes (FIN-S) Stabilized Finite Element Flow Solve", Computers & Fluids, Vol. 15, No. 4, pp. 281–292, (2014).

[9] Doustdar, M.M., Mardani, M.M., and Ghadak, F., "Aero-heating Modelling on the Ablative Noses during Flight Trajectory", Aircraft Engineering and Aerospace Technology Journal, In Press, (2017).

[10] Doustar, M.M., Mardani, M., and Ghadak, F., " Investigation of Wall Catalytic Effects on the Aeroheation of Hypersonic Ablative Noses by Space Marching Method", Mechanic and Aerospace Engineering Journal of Imam Hossien University, Vol. 12, No. 1, pp. 15-26, (2017) (in Persian).

[11] Doustar, M.M., Mardani, M., and Ghadak, F., "Simulation of Temperature Distribution for Hypersonic Ablative Noses during Flight Trajectory by Space Marching Method", Modares Mechanical Engineering, Vol. 16, No. 12, pp. 163-174, (2016) (in Persian).

[12] Doustdar, M.M., Mardani, M.M., and and Ghadak, F., " Numerical Simulation of Radiance Effects on the Aerodynamic Heating of Ablative Nose with VSL-VBLS Method", Structure and Fluid Journal of Shahrod University, Vol. 7, No. 1, pp. 175-186, (2017) (in Persian).

[13] Ekert, E.R., "Engineering Relations for Heat Transfer and Friction in High-velocity Laminar and Turbolent Boundral-layer Flow Over Surfaces with Constant Pressure and Temperature", Trans. of the ASME, Vol. 78, No. 6, pp. 1273-1281, (1986).

[14] Zein, T.F., "Heat Transfer in the Melt Layer of a Simple Ablation Model", Journal of Thermophysicsand Heat Transfer, Vol. 13, No. 4, pp. 321-332, (1999).

[15] Rahimi, A.B., "Numerical Modeling of Charring Material Abalation with Considering Chemical Reaction, Mass Transfer and Surface Heat Transfer Effects", Journal of Thermophysicsand Heat Transfer, Vol. 15, No. 5, pp. 214-221, (2010).

[16] Karemian, H., Kafarian, M., and Azezi, M., "Hypersonic Flow Domain Sloution on the Missile Body with Consedering of High Temperature Effects to Calculate of Aeroheating", Research Project, Aerospace Engineering Complex of Amirkabir University, Iran, (2013)(In Persion).

[17] Howard, S., and Walter, E., "Heat-transfer and Pressure Distribution on Six Blunt Noses at a Mach Number of 2", NASA Research Memorandum, Bressette Langley Aeronautical Laboratory NASA, , Vol. 12, No. 4, pp. 21-28, (1975).

[18] Park, C., "Stagnation Point Ablation of Carbonaceous Flat Discs Part I", AIAA Journal, Vol. 21, No. 11, pp. 1588-1594, (1983).

[19] Park, C., "Calculation of Stagnation Point Heat Transfer for Pioneer Venus Probes", Proposed NASA Technical Memorandum, Vol. 8, No. 4, pp. 38-51, (2002).

[20] Emerson, D.R., and John, B., "Investigation of Heat and Mass Transfer in a Lid-driven Cavity under Non-equilibrium Flow Conditions", Numerical Heat Transfer, Part B, Vol. 5, No. 5, pp. 48-62, (2010)

[21] Kumar, A., "Laminar and Turbulent Flow Solutions with Radiation and Ablation Injection for Jovian Entry", AIAA Paper 80-0288, Vol. 12, No. 3, pp. 30-41, (1980).

[22] Reid, C.M., and Prausnitz, S.T., "*The Properties of Gases and Liquids*", McGraw-Hill, New York, (1977).

[23] Bradshaw, P.T., and Whitelaw, J., "Engineering Calculational Methods for Turbulent Flow", Academic Press, Vol. 16, No. 4, pp. 47-62, (1981).

[24] Marvin, J.D., "Turbulence Modeling for Computational Aerodynamics", AIAA Journal, Vol. 21, No. 7, pp. 941-955, (1983).

[25] Lomax, H., and Inouye, M., "Numerical Analysis of Flow Properties about Blunt Bodies Moving at Superonic Speeds in an Equilibrium Gas", NASA TR-R-204, Vol. 12, No. 5, pp. 54-70, (1964).

[26] Zhluktov, S.V., “Viscous Shock Layer Simulation of Airflow Past Ablating Blunt Body with Carbon Surface”, Journal of Thermo Physics and Heat Transfer Vol. 13, No. 1, pp. 442-462, (1999) .

Nomenclature

C	=	Concentration
Cn_i	=	Coefficients of numerical derivatives
CR_i, DR_i	=	Constant of air chemical reactions

dt = Time step (s)

dy = Distance between two elements (m)

EL = Number of ions in reactions of air

f = Surface function

j = Index to defining the type of body

J = Specific mass flux

k = Iteration counter

K = thermal conductivity (w/m^2k^0)

k_{br} = Backward chemical reactions rate

k_v = Radiation coefficient

k_{fr} = Forward chemical reactions rate

H = Mean curvature for the main body

H_S = Mean curvature for the EAB

l_{br}, l_{fr} = Collective terms of mass action law

M = Molecular weight (kg)

M_i = Catalytic third body

N_{N2} = Nitrogen mole fraction

N_{O2} = Oxygen mole fraction

n_s = Number of species

P_k = Grid scaling

q = Dynamic pressure (Mpa)

q^* = Aerodynamic heating magnitude (w)

q_r = Radiation heat transfer rate

R_n = Blunt radii (m)

Rr = Rate of reaction

s = Curvature distance (m)

St = Stanton number

T = Temperature (k)

u = Tangential velocity (m/s)

U = Free stream velocity (m/s)

v = Normal velocity (m/s)

V_{cs} = Ablator recces rate (m/s)

$\dot{w}_i$ = Source term $(1/s)$

w_i^1, w_i^2 = Source term components $(1/s)$

X_i = Mole fraction

$X_{n_{cs}}$ = Ablator recess

y_{sh} = Shock layer thickness (m)

Z_{j-ns} = Third body efficiency relative to argon

Δh_i^F	=	Formation enthalpy of species
$\Gamma_{ri}^+, \Gamma_{ri}^-$	=	Differences of stoichiometric coefficients
α	=	Angle of attack
$\alpha r, \beta r$	=	Stoichiometric Coefficients
γ	=	Mass concentration of species
δ	=	Convergence criteria of ablation algorithm
ε	=	Convergence criteria of flow solution algorithm
Ξ	=	Reynolds number index
μ	=	Dynamic Viscosity
ζ, η	=	axes of computational coordinates
φ	=	Azimuth angle
ρ	=	density (kg / m^3)
σ	=	Stephan-Boltzmann constant
τ	=	Sheer stress (Mpa)
χ	=	Curvature

Subscripts

0	=	stagnation point
∞	=	free stream
cg	=	gas injected to shock layer due to ablation
ch	=	Char
sh	=	shock
T	=	Eddy
ref	=	reference state
v	=	Virigin

Superscripts

$\_$	=	normalized variables
$*$	=	dimensional variables
$\wedge$	=	tangential and normal components velocity of shock to body

چکیده

هدف از این تحقیق، ارتقاء کد محاسبه کننده ی توزیع دمایی و گرمایش ایرودینامیکی با عنوان CTCA برای دماغه های نامتقارن فناشونده و یا دماغه های با مقاطع غیر حلقوی با استفاده از تئوری ایجاد بدنه متقارن یا EAB است. این کد بوسیله محققین تحقیق فعلی تدوین شده است و نتایج آن بوسیله نتایج آزمایشات پروازی متعدد صحه گذاری گردید. در حالت وجود زاویه حمله و فناشوندگی نامتقارن سطح برای هر کدام از سطوح نصف النهاری، صفحه نصف النهاری معادل ایجاد می گردد. ترکیبی از صفحات نصف النهاری معادل EAB را تشکیل می دهند. با استفاده از سنتیک نامتعادل واکنشهای شیمیایی لایه شوک، معادلات حاکم برای EAB حل و نتایج آن بر روی بدنه اصلی نگاشت می گردد.
نتایج حل مربوط به یک دماغه نوعی در طی مسیر پرواز نشان داد که همگرایی این روش نسبت به روشهای مبتنی بر حل گرهای نرم افزار فلوئنت یا UDF بسیار سریعتر است. نتایج این روش با استفاده از روشهای مبتنی بر حل گرهای نرم افزار فلوئنت صحه گذاری شد و خطای نسبی آن کمتر از ۱۰ درصد است.